Chinese Journal of Chemical Engineering 53 (2023) 361–373

Contents lists available at ScienceDirect

Chinese Journal of Chemical Engineering

journal homepage: www.elsevier.com/locate/CJChE

Full Length Article

# Numerical study on the hydrodynamics behavior of a central insert microchannel

Yongbo Zhou, Yang Jin *, Jun Li, Qinyan Wang, Ming Chen

*Engineering Research Center of Comprehensive Utilization and Clean Processing of Phosphorus Resources, School of Chemical Engineering, Sichuan University, Chengdu 610065, China*

A R T I C L E I N F O

*Article history:*
Received 12 September 2021
Received in revised form 17 January 2022
Accepted 19 January 2022
Available online 31 January 2022

*Keywords:*
Microchannel
Process intensification
Computational fluid dynamics
Liquid–liquid flow pattern
Central insert

A B S T R A C T

In this work, the computational fluid dynamics method is used to study the liquid hydrodynamics behavior in the microchannel without central insert (MC1) and the central insert microchannel (MC2), respectively. The maximum deviation between simulation and experiment is 24%. The formations of flow patterns are explained based on contours and force analysis where the flow pattern maps are established by two-phase flow rate. The effects of aqueous phase viscosity and two-phase flow rate on the characteristic sizes of each flow pattern are also explored. Specifically, four unconventional flow patterns are found in MC2, namely the unique droplet flow, the unique slug flow, the unique coarse annular flow and the unique film annular flow. Though the insert occupies part of the channel, the pressure difference in the channel is significantly reduced compared with MC1. Moreover, the insert significantly changes the formation velocity range of each flow pattern, greatly broadens the formation range of annular flow and also has an important influence on the characteristic size of the flow pattern. The organic-phase dimensionless axial size ($L_o/W$) and the dimensionless radial size ($D_o/W$) of the droplet (slug) are negatively related to the aqueous-phase viscosity ($\mu_a$) and flow rate ($u_a$). The $D_o/W$ of the annular is negatively correlated with $\mu_a$ and positively correlated with organic-phase flow rate ($u_o$). This study provides direct numerical evidence that the insert is key to the formation of bicontinuous phase flow pattern, as well as further strengthens our understanding of the flow characteristics and optimization design of insert microchannels.



## 1. Introduction

In recent decades, ever-growing attention has been paid to microfluidic systems due to their outstanding features such as smaller volume, higher security, easier controlling and superior heat and mass transfer performance. Its applications have been extended to the fields of chemistry, materials, chemical industry, environment and energy [1–4]. For the mass transfer or reaction process in the microchannel, the flow pattern is the basis for studying two-phase flow and mass transfer characteristics. The optimization of the two-phase flow pattern is the key to further strengthening the microreactor transfer process.

Table 1 briefly summarizes two-phase flow patterns of microchannels in published literature. Kashid *et al.* [5] studied the influence of the microchannel inlet shape and cross-sectional shape on the two-phase flow patterns, and observed slug flow, droplet flow, deformed interface flow, *etc.* Cherlo *et al.* [8] and Darekar *et al.* [11] studied the influence of two-phase physical properties on the two-phase flow patterns and observed slug flow, droplet flow, parallel flow, *etc.* In addition, there are researchers studying the influence of the internal structure of the microchannel on the two-phase flow. Yin *et al.* [15] constructed staggered rectangular baffles in T-shaped microchannels to disperse the slug flow into slug droplets. Verma *et al.* [16] added stainless steel inserts to the serpentine channel to disperse the slug flow and droplet flow into smaller intermittent slug flow and droplet-dispersed flow. On the one hand, we find that most of the research focus in the above literature is on dispersed flow patterns, such as slug flow and droplet flow, because dispersed flow patterns can increase the contact area between the two phases and improve the mass transfer rate [18]. However, the great dispersion of one phase will make it difficult to coalesce and lead to difficult phase separation, even emulsification phenomenon [19]. On the other hand, we find that there are few published studies on bicontinuous phases annular flow, which has higher mass transfer rate. Because in conventional microchannels, the formation range of annular flow is small, and the internal phase will deviate from the center, and

* Corresponding author.
*E-mail address:* jinyangyoung@scu.edu.cn (Y. Jin).

https://doi.org/10.1016/j.cjche.2022.01.019
1004-9541/

**Table 1**
A brief summary of microfluidic flow patterns in published literature

| Ref. | Microchannel type; dimension/mm | Continuous phase–dispersed phase system | Parameters varied | Flow pattern |
|---|---|---|---|---|
| Kashid *et al.* [5] | T, Y, co-axial; square and trapezoidal: $d_h$ = 0.27, 0.40 | Water–toluene | Flow rates of two phases, microchannel geometry | Slug, slug-droplet, annular, parallel, deformed interface flow |
| Jovanovic *et al.* [6] | Y; circular: $d$ = 0.25 | Water–toluene | Flow rates and phase ratio of two phases, channel length | Annular, bubbly, parallel, slug flow |
| Zhao *et al.* [7] | T; rectangular: $d_h$ = 0.40 | Water–kerosene | Flow rates of two phases | Slug, droplet, parallel, annular flow |
| Cherlo *et al.* [8] | T; rectangular and square: $d_h$ = 0.54,1.0 | Water–kerosene, hexanol, octane, coconut oil | Flow rates of two phases, channel sizes, and several fluid systems | Slug flow and stratified flow |
| Xu *et al.* [9] | T; $h \times w = 0.15 \times 0.2$, $d_i$ = 0.04 | SDS–*n*-octane | Flow rates of two phases, interfacial tension, contact angle | Laminar, plug, cobble, droplet flow |
| Fu *et al.* [10] | T; $h \times w = 0.4 \times 0.4, 0.4 \times 0.6, 0.4 \times 0.8$ | CMC solutions–cyclohexane | Microchannel dimensions, flow rates of two phases, the concentration of CMC solutions | Slug, droplet, jetting, parallel flow |
| Darekar *et al.* [11] | Y; $d_h$ = 0.26, 0.76 | *n*-butanol–water, *n*-butyl acetate–water, toluene–water | Microchannel diameters, flow rates, interfacial tension of two phases | Slug, droplet, slug-droplet, parallel flow |
| Wu *et al.*[12] | Cross-shaped; square: $d_h$ = 0.20, 0.40, and 0.60 | Water–butanol, hexane, toluene, oil | Microchannel sizes, flow rates and physical properties of two phases | Tubing/threading, dripping, jetting |
| Foroughi *et al.* [13] | Co-axial; circular: $d$ = 0.25 | Silicone oil–water | Flow rates of two phases | Annular, plug, slug, droplet, annular-droplet flow |
| Lan *et al.*[14] | Co-axial; circular: $d$ = 0.25 | Silicone oil–solutions of poly-sulphone in DMF | Flow rates, viscosities and interfacial tension of two phases | Dripping and jetting flow |
| Yin *et al.*[15] | T-shaped with staggered rectangular baffles: $w$ = 0.4, 0.8 | Water–$CO_2$ | Baffle blockage length, baffle interval, channel width and flow rates of two phases | Slug flow, broken-slug flow |
| Verma *et al.* [16] | Serpentine mini geometry with stainless steel insert: $d$ = 2 mm | Water–toluene, kerosene–water, jatropha oil–methanol | Flow rates of two phases and several fluid systems | Slug, slug-droplet, intermittent slug, droplet-dispersed |
| Lv *et al.* [17] | Butterfly-shaped microreactor: $h \times w = 1.2 \times 0.8$ | Water–butanol | Flow rates and phase ratio of two phases | Droplet, Taylor, stratified, annular, and dispersed flow |

random fluctuations will also appear at the interface of the two phases [20]. We have found experimentally that the introduction of the insert in the co-axial microchannel can form the bicontinuous phase slug flow and droplet flow different from the conventional microchannel, as well as the stable bicontinuous phase annular flow, realizing the bicontinuous two phases flow in the microchannel. It can avoid the contradiction between the mass transfer rate and the phase separation rate in two-phase mass transfer operations, such as liquid–liquid extraction, that is, the mass transfer rate between the two phases is fast enough, but there is no dispersed phase, and the two phases separate quickly. Therefore, it is necessary to conduct a detailed study on the two-phase flow characteristics of the insert microchannel.

Plugging insert into microchannels is a challenge. Experimental manipulation is relatively difficult, and details of flow pattern generation and transformation, such as velocity vector size and direction, and phase interface changes, are difficult to obtain under the microscope. Previous studies have shown that, volume of fluid (VOF), as an economical and efficient technology, can effectively solve the problems existing in experiments, and has been widely used in the study of two-phase flow, heat and mass transfer in micro-reaction systems. Ghaini *et al.* [21] proved that the liquid film on the wall of the microchannel formed by two phases would have an effect on the flow, and the internal circulation in the slug was the most important effect. Kashid *et al.* [22] studied the flow characteristics and mass transfer between two adjacent slugs by VOF method, and found that the internal circulation can promote the mass transfer in the phase. Lan *et al.* [14] studied the formation mechanism of dripping and jetting flow in co-axial microchannels by VOF and experiments, and revealed the kinetics of droplet formation. Abdollahi *et al.* [23] studied the pressure drop and film thickness of slug flow in square microchannels by experiments combined with VOF, and established a mathematical model to predict the film thickness and pressure drop. Li *et al.* [24] studied the hydrodynamic characteristics in microchannels by means of experiments and VOF. The slug film thickness, slug velocity and slug length were measured and compared with the mathematical models established by other scholars. The results are in good agreement with each other.

The purpose of this work is to investigate the effect of central insert on dynamic behavior of liquid–liquid flows. To investigate this, the VOF method is chosen. The formation of each flow pattern in the co-axial insert microchannel is studied, and compared with that in the conventional co-axial microchannel. The influence of insert on the formation and characteristics of bicontinuous phase flow pattern is clarified, and the flow pattern map with two-phase flow rate as coordinate axis is established. In addition, this work also studied the influence of aqueous viscosity and two-phase flow rate on the characteristic dimensions of each flow pattern. This work is conducive to solving the contradictory relationship between the mass transfer rate and the phase separation rate in the extraction process.

## 2. Simulation Method

### 2.1. VOF method

The VOF method is a surface tracking method based on a fixed Euler mesh. It is based on the assumption that the two phases are incompressible and cannot be permeated or mixed with each other [25]. In the VOF method, the share of the fluid $i$ in the mesh can be described by the volume fraction $\alpha_i$. $\alpha_i = 0$ indicates that there is no fluid $i$ in the mesh, $0 < \alpha_i < 1$ indicates that the mesh contains the phase interface, and $\alpha_i = 1$ indicates that the mesh is filled with fluid $i$. The two-phase flow in the microchannel involves the interaction between the immiscible two phases, which are coupled by phase volume fraction $\alpha$. And the sum of the volume fractions of the two fluids in each mesh of the computational model is 1:

$$\alpha_a + \alpha_o = 1 \tag{1}$$

Among them, $\alpha_a$ and $\alpha_o$ are the volume fractions of aqueous phase and organic phase fluid, respectively.

In the whole flow field calculation region, immiscible two phases use the same phase equation:

$$\frac{\partial \alpha}{\partial t} + \nabla \cdot (\alpha \boldsymbol{U}) = 0 \tag{2}$$

where $t$ is time and $\boldsymbol{U}$ is fluid velocity field.

The continuity equation and momentum equation of the immiscible two phases are as follows:

$$\nabla \cdot \boldsymbol{U} = 0 \tag{3}$$

$$\frac{\partial(\rho \boldsymbol{U})}{\partial t} + \nabla \cdot (\rho \boldsymbol{U}\boldsymbol{U}) = -\nabla p + \nabla \cdot \left[\mu\left(\nabla \boldsymbol{U} + \nabla \boldsymbol{U}^{\mathrm{T}}\right)\right] + \boldsymbol{F}_{\mathrm{v}} \tag{4}$$

where $p$ is the pressure, $\rho$ and $\mu$ are the density and viscosity, and $\boldsymbol{F}_{\mathrm{v}}$ is the source term. In the calculation area, the density, viscosity and source term are as follows:

$$\rho = \alpha_a \rho_a + \alpha_o \rho_o \tag{5}$$

$$\mu = \alpha_a \mu_a + \alpha_o \mu_o \tag{6}$$

$$\boldsymbol{F}_{\mathrm{v}} = \rho \boldsymbol{g} + \boldsymbol{F}_{\mathrm{s}} \tag{7}$$

where $\rho_a$ and $\rho_o$ are the densities of aqueous phase and organic phase respectively, and $\mu_a$ and $\mu_o$ are the viscosity of aqueous phase and organic phase, respectively. $\boldsymbol{g}$ is the gravity acceleration, and $\boldsymbol{F}_{\mathrm{s}}$ is the surface tension.

The size of the microchannel in this study is sub-millimeter, thus the channel size is small and the density of the two-phase fluid is not much different, so the gravity term $g$ in the source term $\boldsymbol{F}_{\mathrm{v}}$ can be ignored. In the VOF method, the continuous surface force model (CSF) [26] is usually used to characterize the interface force between the two phases. In the CSF model, the surface tension is regarded as a volume force acting on the fluid in the mesh element in the phase interface region, which can be characterized as a function of the interfacial tension coefficient and the interface shape:

$$\boldsymbol{F}_{\mathrm{s}} = \sigma \kappa \nabla \alpha \tag{8}$$

where $\sigma$ is the interfacial tension coefficient. $\kappa$ is the mean curvature of the interface, and its calculation formula is as follows:

$$\kappa = \nabla \cdot \hat{\boldsymbol{n}} = \frac{1}{|\boldsymbol{n}|}\left[\left(\frac{\boldsymbol{n}}{|\boldsymbol{n}| \cdot \nabla}\right)|\boldsymbol{n}| - (\nabla \cdot \boldsymbol{n})\right] \tag{9}$$

where $\hat{\boldsymbol{n}}$ is the unit normal vector.

The inlet flow rate of aqueous phase and organic phase is defined as follows:

$$u_a = \frac{Q_a}{A_a} \tag{10}$$

$$u_o = \frac{Q_o}{A_o} \tag{11}$$

Among them, $Q_a$ and $Q_o$ are the volume flow rates of aqueous phase and organic phase, respectively. $A_a$ and $A_o$ are the cross-sectional area of the entrance channel of the aqueous phase and organic phase, respectively.

### 2.2. Geometry and mesh model

Graphs of the experimental device are shown in Fig. 1. Microchannel is made in quartz with an outer diameter of 3 mm, an inner diameter of 0.9 mm and a length of 150 mm. The outer diameter of the stainless steel capillary tube is 0.5 mm, the inner diameter is 0.3 mm and the length is 2 cm. The insert consists of a narrow-diameter $W_{\mathrm{ins,nd}}$ = 0.26 mm, wide-diameter $W_{\mathrm{ins,wd}}$ = 0.36 mm, length $L_{\mathrm{ins}}$ = 1 mm "bead string" periodic arrangement, which is placed in the center of the microchannel. The organic phase fluid enters a stainless steel capillary through the organic phase inlet on one side, and is then led into the quartz capillary, while the aqueous phase fluid flows directly into the quartz capillary from the aqueous phase inlet. In Fig. 2, the models used for numerical calculation are co-axial microchannel (MC1) and insert co-axial microchannel (MC2) without considering wall thickness. Organic phase entrance channel's inner diameter $W_{\mathrm{in,o}}$ = 0.5 mm, length $L_{\mathrm{in,o}}$ = 2 mm. Microchannel's main channel inner diameter $W$ = 0.9 mm, length $L$ = 20 mm.

### 2.3. Boundary conditions and numerical methods

The simulated two-phase fluids are toluene and water (glycerol is used to change the viscosity of the aqueous phase). The physical parameters of the fluid are experimentally measured at 25 °C, as shown in Table 2. Densities of the liquids were estimated by using specific gravity bottle. Viscosities of the liquids were measured by the Ubbelohde viscometer. Interfacial tensions of the two phases were tested by platinum ring method using an automatic surface tension meter (BZY-201, Shanghai Fangrui Instrument Co., Ltd., China). In the solver, the two-phase entrance condition is defined as velocity inlet and exit condition is defined as outflow. All wall conditions are non-slip static walls, and the maximum Courant number is set to 0.25, so as to control the time step without reducing the simulation quality and accuracy.

In the VOF model, the governing equation is solved by the finite volume difference method, and different components share a set of momentum equations, and the volume ratio occupied by each fluid component is recorded in each calculation unit of the whole flow field. Pressure-implicit with splitting of operators (PISO) is used as the pressure–velocity correlation algorithm, body force weighted scheme is used to interpolate pressure, second-order upwind scheme is used to discretize the momentum equation, and geo-reconstruct scheme based on segmented interface calculation (PLIC) method is used to reconstruct the liquid–liquid interface. After the differential equations are discretized into linear algebraic equations, the Gauss–Seidel method is used to solve them iteratively. The under relaxation factors used in iterative calculation are pressure term 0.3, density term 1, volume force source term 1, momentum source term 0.7. The initialization is standard initialization, the time step is set to $10^{-5}$ s, and each step is iterated 20 times to ensure the simulation accuracy.

## 3. Results and Discussion

### 3.1. Mesh independence and method validity verification

The geometric model is regular, so we can easily generate hexahedral mesh by using node partition method and improve the aspect ratio [27]. To determine the appropriate cell size for the simulations, meshes of different densities are tested. Maximum axial mesh sizes of 200, 100, 66, 50, 40, 33 and 25 μm are considered for the mesh independence analysis. The rule for determining the size of organic phase in MC1 and MC2 is shown in Fig. 3. The organic droplet (slug) in MC1 is completely dispersed, so the axial

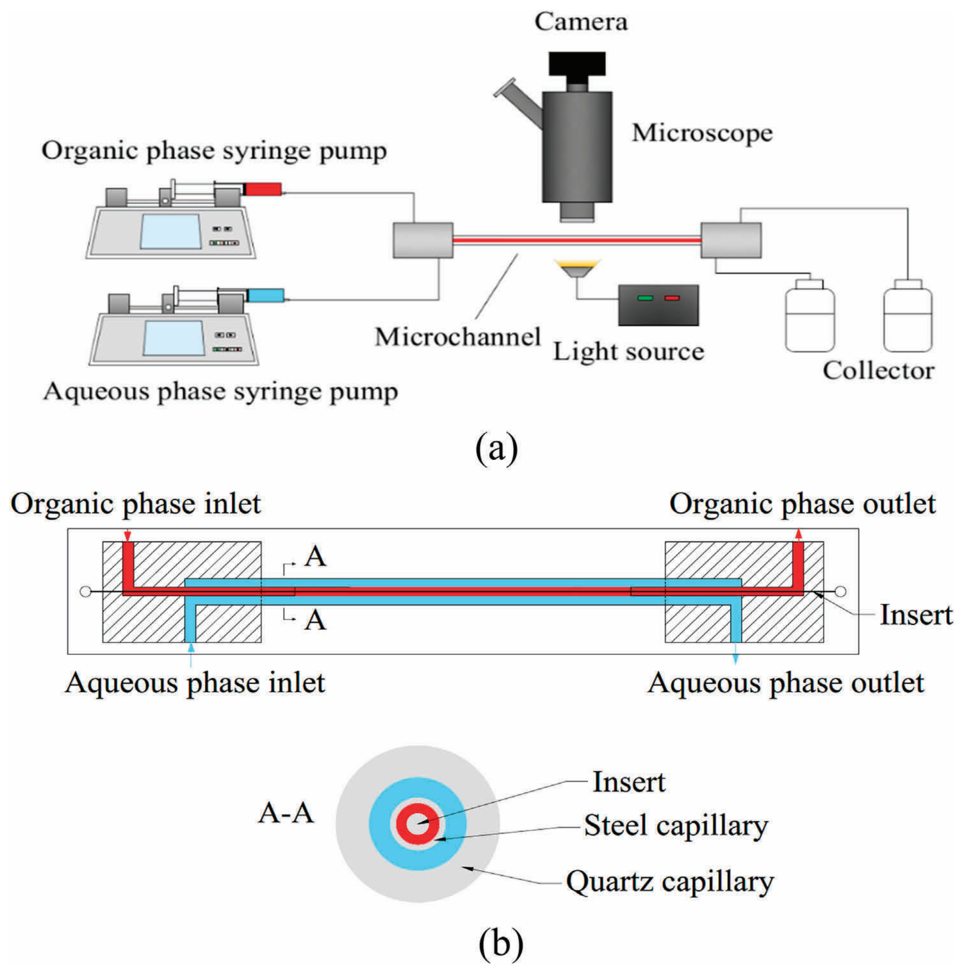


**Fig. 1.** The experimental device used for flow visualization of the two-phase flow patterns: (a) experiment device schematic graph; (b) microchannel schematic graph. In cross section A-A, blue represents aqueous phase inlet, red represents organic phase entrance, and gray represents wall.

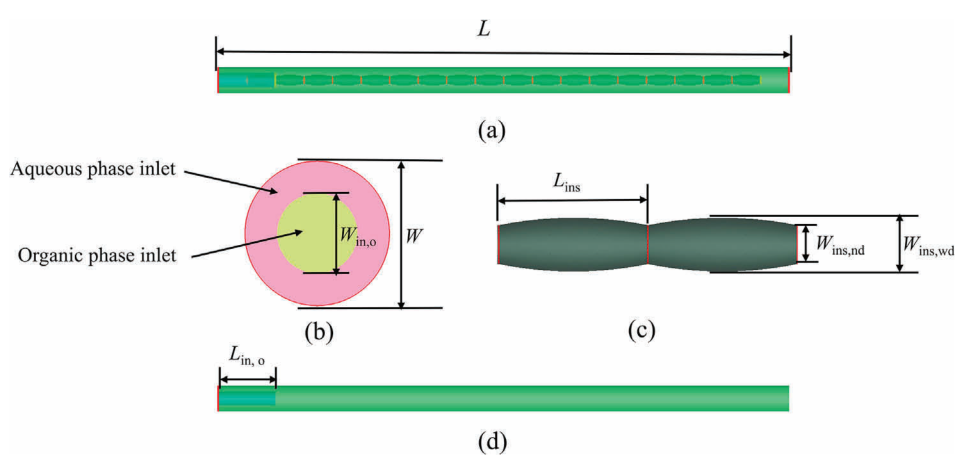


**Fig. 2.** Microchannel CFD simulation geometry: (a) MC2; (b) aqueous inlet and organic inlet; (c) unit insert; (d) MC1.

length is defined as $L_o$, and the radial width is defined as $D_o$. The organic liquid film is connected between the droplet (slug) in MC2, because it is not a dispersed phase in the traditional sense, so a "shuttle" is used as a unit to define the axial length $L_o$ and radial width $D_o$ of the organic phase. The radial width of the organic phase in the annular flow is expressed by $D_o'$, which is expressed as the average of the width $D_1$ at the shortest point of the insert and the width $D_2$ at the widest part of the insert. The aqueous phase flow rate was $u_a = 0.06\ m{\cdot}s^{-1}$, and the organic phase flow rate was $u_o = 0.12\ m{\cdot}s^{-1}$. Organic slug length and aqueous slug length are tested in Table 3. The rough mesh will form a rough and unstable phase interface, which will cause the result to be

**Table 2**
Physical properties of two phases used in this study (25 °C, 0.1 MPa)

| Fluid | $\rho$/g·cm$^{-3}$ | $\mu$/mPa·s | $\sigma$/mN·m$^{-1}$ |
|---|---|---|---|
| Toluene | 0.861 | 0.53 | – |
| Water | 0.996 | 0.95 | 36.1 |
| Water + 10% glycerol | 1.021 | 1.15 | 31.5 |
| Water + 20% glycerol | 1.046 | 1.54 | 29.7 |
| Water + 30% glycerol | 1.071 | 2.16 | 28.2 |
| Water + 40% glycerol | 1.097 | 3.18 | 27.3 |
| Water + 50% glycerol | 1.124 | 5.04 | 26.6 |

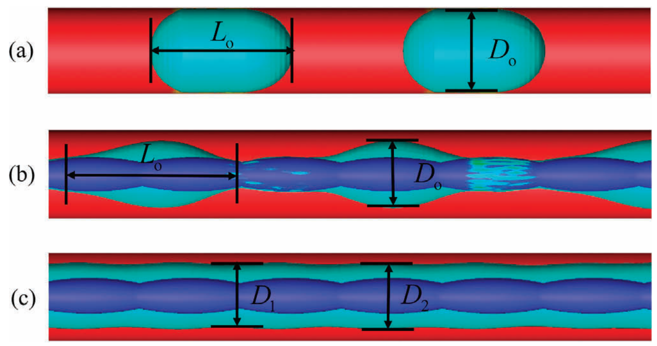


**Fig. 3.** Feature size definition schematic graphs: (a) the axial length and radial width of droplets (slugs) in MC1; (b) the axial length and radial width of droplets (slugs) in MC2; (c) the radial width of annular flow in MC2.

greatly deviated from the true value. It is verified that when the number of MC1 meshes reaches 1210000 and the number of MC2 meshes reaches 800000, the interface between the two phases in the microchannel is clear, and the result of repeated operation of the same flow pattern is stable. Therefore, in order to save computing time and resources, the mesh models with global mesh number of 1210000 for MC1 and 800000 for MC2 are selected for follow-up research.

In order to verify the effectiveness of the simulation method, the flow patterns' sizes obtained from the experiment and simulation were compared. As shown in Fig. 4, it can be seen that the simulation results are basically consistent with the experimental results. The maximum deviation of $D_o/W$ is 24%, and the maximum deviation of $L_o/W$ is 17.6%, which lays a foundation for the subsequent simulation research.

### 3.2. Type of flow pattern

Figs. 5 and 6 show the flow patterns graphs of simulation (left) and experiment (right) in MC1 and MC2. It is observed that there are three flow patterns in MC1 namely, droplet flow (DF), slug flow (SF) and annular flow (AF) (Fig. 5(a)–(c)), which are consistent with the flow patterns reported by Kashid *et al.* [5]. And four flow patterns were observed in MC2, namely, the unique droplet flow (UNI-DF), the unique slug flow (UNI-SF), the unique coarse annular flow (UNI-CAF) and the unique film annular flow (UNI-FAF) (Fig. 6(a)–(d)). In the case of insert, the shapes of MC2's flow patterns are different from the flow patterns reported in Refs. [28,29]. We compare the four flow patterns formed by MC2 with those formed by MC1 and define them as follows. UNI-SF is a slug flow with a dimensionless width $D_o/W > 0.8$ at the center of the organic phase slug, while UNI-DF is a droplet flow with a dimensionless width $D_o/W < 0.8$ at the center of the organic phase droplet. UNI-CAF is one type of annular flow with organic phase

**Table 3**
Mesh independence verification of this work

| Maximum axial mesh size/μm | MC1 | | | MC2 | | |
|---|---|---|---|---|---|---|
| | Mesh number | Organic slug length/μm | Aqueous slug length/μm | Mesh number | Organic slug length/μm | Aqueous slug length/μm |
| 200 | 298000 | 1424 | 1055 | 199000 | 1801 | 588 |
| 100 | 673000 | 1488 | 1031 | 402000 | 1845 | 605 |
| 66 | 907000 | 1526 | 1025 | 599000 | 1891 | 631 |
| 50 | 1210000 | 1587 | 1002 | 800000 | 1925 | 648 |
| 40 | 1516000 | 1601 | 998 | 1004000 | 1929 | 645 |
| 33 | 1821000 | 1612 | 998 | 1201000 | 1931 | 648 |
| 25 | 2430000 | 1629 | 988 | 1602000 | 1928 | 655 |

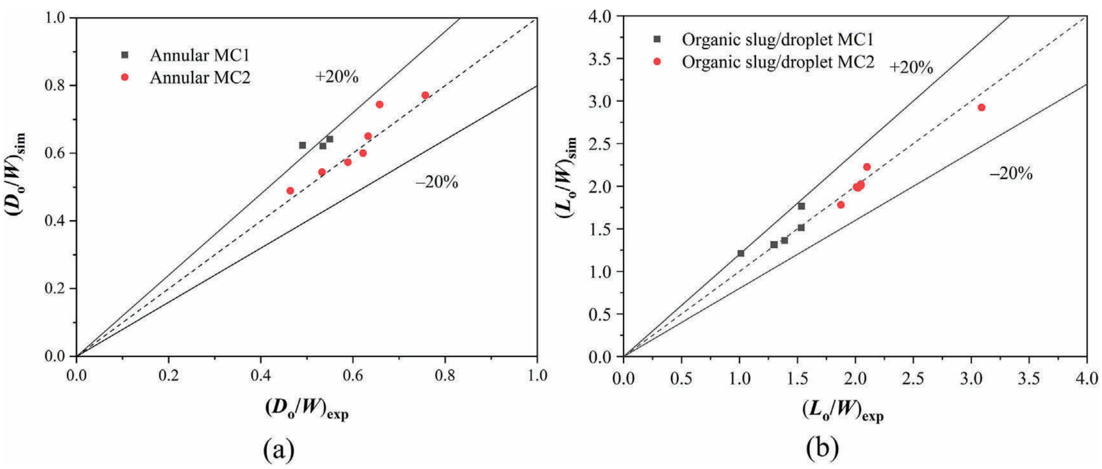


**Fig. 4.** Comparison of flow pattern characteristic sizes between experiment and simulation: (a) $D_o/W$; (b) $L_o/W$.

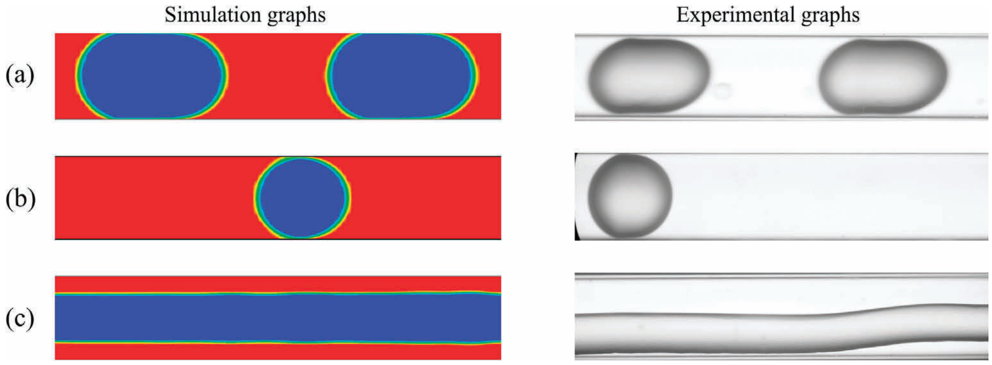


**Fig. 5.** Simulation and experimental graphs of flow patterns in MC1: (a) $u_a = 0.06\ m\cdot s^{-1}$, $u_o = 0.12\ m\cdot s^{-1}$, SF; (b) $u_a = 0.1\ m\cdot s^{-1}$, $u_o = 0.02\ m\cdot s^{-1}$, DF; (c) $u_a = 0.1\ m\cdot s^{-1}$, $u_o = 0.25\ m\cdot s^{-1}$, AF. Blue represents the organic phase and red represents the aqueous phase.

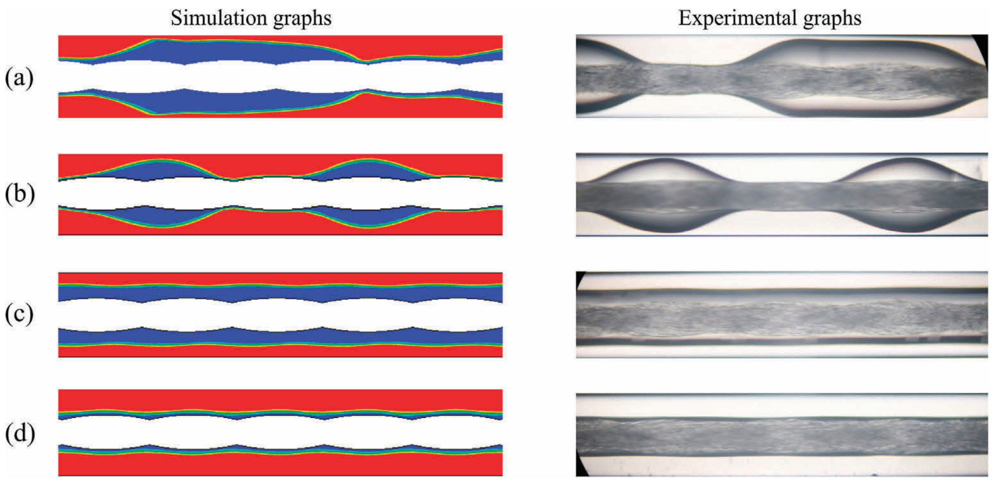


**Fig. 6.** Simulation and experimental graphs of flow patterns in MC2: (a) $u_a = 0.02\ m\cdot s^{-1}$, $u_o = 0.1\ m\cdot s^{-1}$, UNI-SF; (b) $u_a = 0.02\ m\cdot s^{-1}$, $u_o = 0.04\ m\cdot s^{-1}$, UNI-DF; (c) $u_a = 0.02\ m\cdot s^{-1}$, $u_o = 0.2\ m\cdot s^{-1}$, UNI-CAF; (d) $u_a = 0.2\ m\cdot s^{-1}$, $u_o = 0.02\ m\cdot s^{-1}$, UNI-FAF. Blue represents the organic phase and red represents the aqueous phase.

dimensionless width $D_o/W > 0.5$, while UNI-FAF is one type of annular flow with organic phase dimensionless width $D_o/W < 0.5$. As can be seen in Fig. 6(a) and (b), UNI-DF and UNI-SF are not completely dispersed, but are connected by anorganic liquid film on the surface of the insert. In Fig. 6(c), the flow of the UNI-CAF, aqueous phase in the annular region between the channel wall and the organic liquid column is observed. The UNI-FAF formed in Fig. 6(d) is the flow pattern of liquid film surrounding the insert. The insert enables the above two annular flows to be fixed in the center of the channel without deviation, and the flow pattern can be kept stable without disorder even if the difference between the two-phase flow velocities are 10 times. This is also the reason why the annular flow formed in MC2 is more stable than the AF observed by MC1 and other scholars [20,28]. The regularly deformed insert makes the organic liquid column form a regularly deformed phase interface, which is helpful to the formation of the recirculation flow [30].

It can be seen that the experiment and simulation have achieved good consistency. However, there are still some differences. The simulated slug in MC1 is slightly larger than the experimental slug and the simulated annular flow in MC1 is slightly wider than that in the experiment. In the experiment, MC1's annular flow was not always in the middle of the channel. The connecting liquid film between slugs of MC2 is difficult to capture in experiment graphs. Because there are observation errors in the experiment, and the experimental device has a certain roughness compared with the simulation model's smooth wall surface.

### 3.3. Analysis of flow pattern formation

#### 3.3.1. Annular flow formation

Fig. 7 shows the annular flow formation process of MC1 and MC2. In MC1, the head of the blue organic phase flows out from the organic phase channel to the main channel and expands. When the organic phase head flows out, the organic phase flows in the central area of the main channel, forming a long liquid column surrounded by aqueous phase. The width of the head of the organic phase liquid column is slightly larger than that of the main body of the liquid column, and the width of the main body of the liquid column is basically constant after stabilization. As shown in Fig. 7 (b), during the formation of UNI-CAF, the head of the organic phase entering the main channel expands, almost occupying the whole channel, and the attachment of the insert makes it unable to occupy the main channel completely, so the main body width of the organic phase gradually decreases from behind the head, and then remains stable. As shown in Fig. 7(c), in MC2, when forming UNI-FAF, the flow rate of the organic phase is very small. The head of the organic phase expands slightly into the main channel, and the aqueous phase cannot cut off the organic phase, but squeezes the organic phase into a thin liquid film, which is attached to the surface of the insert.

#### 3.3.2. Slug/droplet's formation

Fig. 8(a) and (b) show the formation of organic slug in MC1 and MC2, respectively. When the organic phase flows from the organic phase channel to the main channel, two flow modes of dripping flow and jetting flow will be formed. Utada [31] and Lan [14] defined and studied these two modes. In this work, the two-phase flow rate was maintained to make the formed slug in dripping mode. For conventional microchannels, the formation process of an organic slug can be divided into four steps: emergence, expansion, extrusion and necking. After that, the third and fourth steps are repeated, and the neck of the organic phase breaks and retracts periodically to form slugs one by one. The formation process of the slug in MC2 is roughly the same as that of MC1, however there are some differences. In MC2, the head of the organic phase flowing out in the second step becomes fusiform by the surface force of the insert (which is analyzed in detail in the next section), and the necking process no longer forms a fractured dispersed phase slug like MC1, but forms a continuous phase slug connected by the liquid film on the surface of the insert.

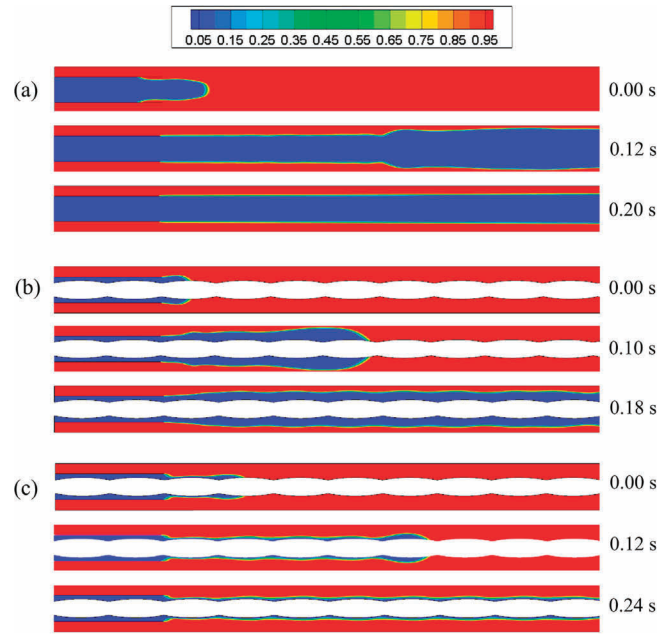


**Fig. 7.** The annular flow formation graphs: (a) MC1, $u_a$ = 0.1 m·s$^{-1}$, $u_o$ = 0.3 m·s$^{-1}$; (b) MC2, $u_a$ = 0.1 m·s$^{-1}$, $u_o$ = 0.3 m·s$^{-1}$; (c) MC2, $u_a$ = 0.25 m·s$^{-1}$, $u_o$ = 0.05 m·s$^{-1}$. Blue represents the organic phase and red represents the aqueous phase.

Fig. 9 shows the formation of organic droplets. In MC1, the formation process of the droplet is similar to that of the slug: the head of the organic phase expands outward at the main channel, and then the neck is sheared by the aqueous phase with higher velocity, so that it breaks into droplets before it lengthens significantly and fills the main channel, so the volume of the droplet is much smaller than that of the slug. In MC2, droplets are formed in the same way as slugs, because there is no fracture process, so usually one droplet is not fully formed before the next droplet is formed.

### 3.3.3. Velocity field and force analysis of slug flow

Take the formation of slug flow as an example, Fig. 10 shows the velocity vectors of the initial formation of a slug in MC1 and MC2. As can be seen in Fig. 10(a), two velocity vector vortexes in MC1 are formed when the organic phase is broken and retracted. At the moment of the fracture of organic phase, the interfacial tension of the two phases and the influx of the aqueous phase at the fracture together cause the change of the direction of the velocity vector of the aqueous phase, thus forming a velocity vector vortex. The periodic fracture of the organic phase promotes the periodic formation of the vortex in the aqueous phase, and the periodic formation of the vortex in the aqueous phase squeezes the fracture of the

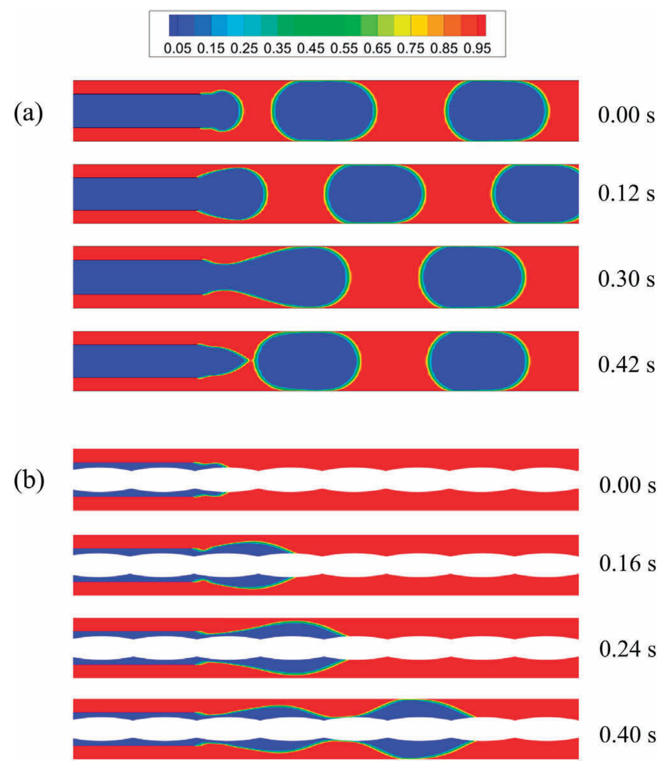


**Fig. 8.** The formation process of slugs: (a) MC1, $u_a$ = 0.06 m·s$^{-1}$, $u_o$ = 0.12 m·s$^{-1}$; (b) MC2, $u_a$ = 0.06 m·s$^{-1}$, $u_o$ = 0.12 m·s$^{-1}$. Blue represents the organic phase and red represents the aqueous phase.

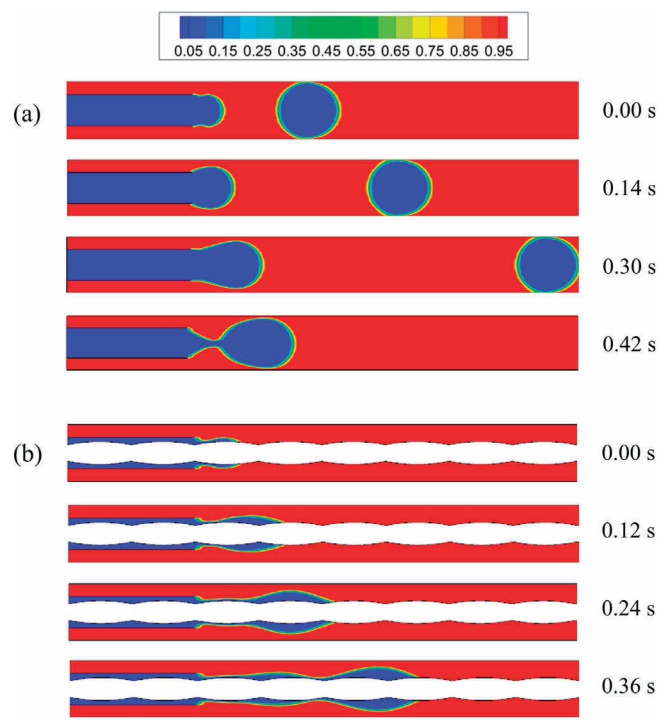


**Fig. 9.** The formation process of droplets: (a) MC1, $u_a$ = 0.12 m·s$^{-1}$, $u_o$ = 0.06 m·s$^{-1}$; (b) MC2, $u_a$ = 0.12 m·s$^{-1}$, $u_o$ = 0.06 m·s$^{-1}$. Blue represents the organic phase and red represents the aqueous phase.

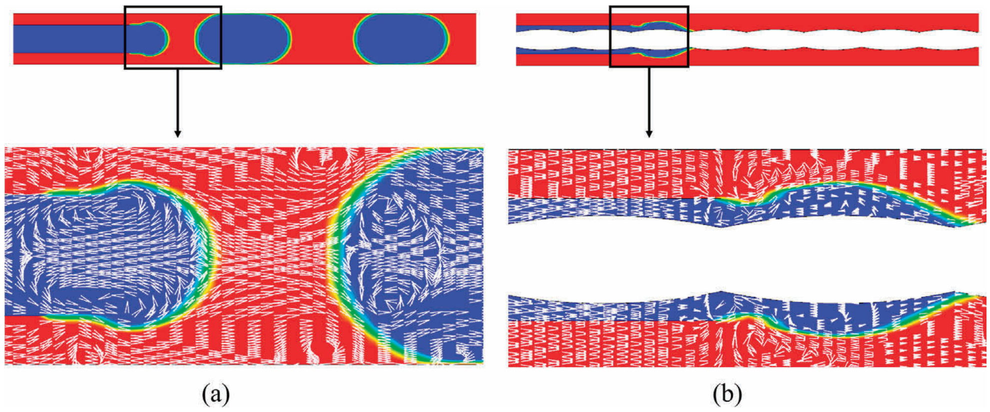


**Fig. 10.** The velocity vector graphs at the formation of the slug: (a) MC1, $u_a$ = 0.06 m·s$^{-1}$, $u_o$ = 0.12 m·s$^{-1}$; (b) MC2, $u_a$ = 0.06 m·s$^{-1}$, $u_o$ = 0.12 m·s$^{-1}$. Blue represents the organic phase and red represents the aqueous phase.

organic phase. This mutual promotion ensures the orderly and stable production of slugs in the organic phase. It can be seen from the previous section that the organic slug formed by MC2 is connected by liquid film and there is no fracture retraction process. Different from the slug in MC1 breaking and shrinking to form a vortex, the vortex in MC2 is formed because the insert provides a regularly deformed attachment surface while occupying part of the main channel space. That makes the superficial velocities of the two phases increase after entering the main channel, and the velocity directions of the two-phase flow on the insert surface are affected a lot by the insert shape and the insert surface force. The change of flow velocities make the disturbance of the insert to the two phases more intense, so that the two phases can form recirculation flows on the surface of the insert [30]. This kind of recirculation flow can be generated anywhere in the channel,

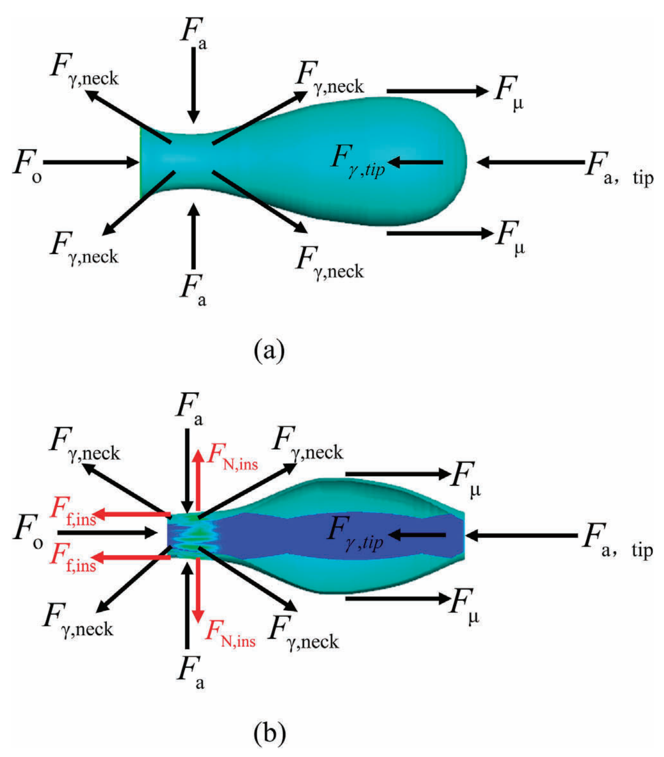


**Fig. 11.** Force analysis graphs of the slug: (a) MC1, $u_a$ = 0.06 m·s$^{-1}$, $u_o$ = 0.12 m·s$^{-1}$; (b) MC2, $u_a$ = 0.06 m·s$^{-1}$, $u_o$ = 0.12 m·s$^{-1}$. Light green represents the organic phase, blue represents the insert.

which can effectively enhance the transfer behavior of the two phases.

The qualitative analysis of the force is carried out on the isosurface graph of the slug, as shown in Fig. 11. No matter in MC1 or MC2, the junction of the organic phase will be subjected to the pressure of the aqueous phase $F_a$, and the pressure of the main body of the organic phase $F_o$. The neck of the organic slug will be subjected to the two-phase interfacial tension $F_{\gamma,neck}$. The head of organic slug will be subjected to the two-phase interfacial tension $F_{\gamma,tip}$, the pressure of aqueous phase $F_{a,tip}$, and the viscous force $F_\mu$ [32] of aqueous phase relative to the organic phase.

In MC1, when the slug is formed in the fourth step, the force balance is broken by the necking fracture process, and the $F_{\gamma,neck}$ will change sharply. Affected by the interfacial tension between the two phases, the neck of the organic phase immediately retracts to form a complete slug. While in MC2, due to the existence of insert, the molecular cohesion of organic phase is less than thesurface force between organic phase and insert. Under the combined action of insert surface's support force $F_{N,ins}$ and insert surface's friction force $F_{f,ins}$, which are antagonistic to aqueous phase positive pressure $F_{\gamma,neck}$ and slug retraction respectively, the head and tail of organic phase are deformed and shuttle-shaped. The fusiform head is not closed and is connected by a thin liquid film of organic phase, thus formingbicontinuous UNI-SF and UNI-DF.

The slug generation process is related to the dynamic pressure in the system. Lan *et al.* [14] found that the pressure at the outlet of the organic phase is an important parameter to explain the slug formation. In order to study the pressure formed by the slug, the pressure monitoring points are set up in MC1, and the coordinates of the monitoring points are (0, 0, 2.5) and (0, 0, 5). The monitoring points in MC2 are (0, 0.18, 2.5) and (0, 0.18, 0.55). The two-phase inlet condition is $Q_a$ = 42.41 ml·h$^{-1}$, and $Q_o$ = 84.82 ml·h$^{-1}$. The pressure change process of forming a complete slug is studied, as shown in Fig. 12. The pressure periods of MC1 and MC2 are 0.32 and 0.29 s, respectively, corresponding to the time for the formation of the slug in the two microchannels. In Fig. 12(a), the pressure shows a peak and decreases sharply, which is the necking fracture stage of the slug in MC1, which is caused by the sharp change of $F_{\gamma,neck}$. There is also a sharp change in pressure in Fig. 12(b), but it can be found that the pressure drop in MC1 is much larger than that in MC2, which can be explained by the incomplete fracture of the slug formed by MC2 and the film connection of organic phase between the slugs, which reduces the pressure drop. Fig. 12(c) and (d) represent the pressure change of the two-phase flow through the main channel monitoring point, respectively. The two-phase slug in MC1 flows alternately through the monitoring point, so

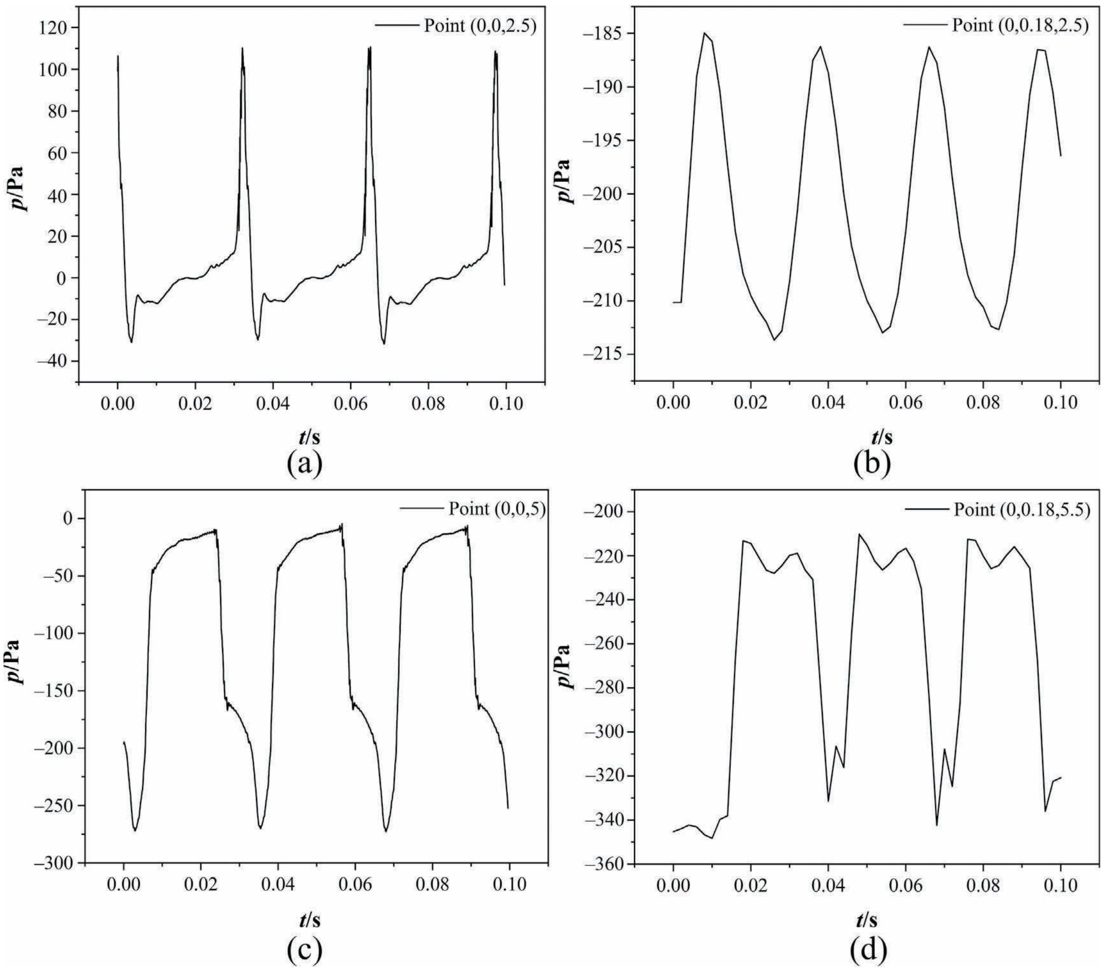


**Fig. 12.** Pressure graphs of monitoring point: (a) MC1 monitoring point (0, 0, 2.5) pressure; (b) MC2 monitoring point (0, 0.18, 2.5) pressure; (c) MC1 monitoring point (0, 0, 5) pressure; (d) MC2 monitoring point (0, 0.18, 5.5) pressure.

the pressure graph is a regular wave graph, while the irregular shape of the insert in MC2 makes the slug phase interface flow through this place periodically and slightly deform, resulting in a periodic slight oscillation of the pressure.

### *3.4. Flow pattern map*

The two-phase flow rate has an important influence on the flow pattern. Based on the results of numerical simulation, the flow pattern maps of MC1 and MC2 are obtained respectively, as shown in Fig. 13(a) and (b). In MC1, AF occupies the upper-left corner of the flow pattern. Because the formation of AF requires a larger $u_o$. With the increase of $u_o$, the $u_a$ range of forming AF expands, so the formation region of AF will extend to the direction of $u_a$ increase with the increase of $u_o$, which is consistent with the conclusion of flow pattern of Wu *et al.* [33]. In MC2, it can be found that the formation region of annular flow is not only at the upper left end of the flow pattern, but also in the large area at the right end of the flow pattern. If there are no broken coordinates, the right half of the flow pattern is completely covered by annular flow. Combined with the force discussed in the previous section, when the inertia force of the aqueous phase cannot overcome the surface force of the insert to shear the organic phase, the organic phase will be attached to the insert to form a liquid film. Therefore, when the $u_o$ is small and remains the same, a continuous increase in $u_a$ will lead to a transition from UNI-SF to UNI-DF and then to UNI-FAF. When the $u_o$ is large, the continuous increase of $u_a$ will lead to the transition from UNI-SF to UNI-CAF. This is because when the $u_a$ is small, the organic phase dominates and the slug is formed. When the inertia force of the organic phase increases to overcome the shearforce of the aqueous phase, UNI-CAF is formed. In addition, it can also be observed that the SF in MC1 is also distributed in the aqueous phase flow rate $u_a = 0.15\ m\cdot s^{-1}$, while the UNI-SF in MC2 is no longer formed when $u_a$ is greater than $0.08\ m\cdot s^{-1}$. On the one hand, because the slug occupies a part of the channel volume, the apparent flow rate in MC2 is greater than MC1 under the same inlet flow rate. On the other hand, the surface force of the slug makes the slug become droplets in $u_a$ to a certain extent. From the overall flow pattern map, the UNI-SF and UNI-DF in MC2 are offset from the formation regionsof SF and DF in MC1, and the annular flow formation region of MC2 is much wider than that of MC1.

### *3.5. Analysis of characteristic size of flow pattern*

The single-factor parameterization studies of flow pattern size provide a deeper understanding of the two-phase flow characteristics. In this part, the numerical simulation method is used to study the effects of two-phase flow rate, insert and aqueous phase viscosity on the axial and radial size of droplet (slug) and radial size of annular flow. The results are taken as the average value of three measurements.

$q$ is defined as the ratio of volume flow rate of aqueous phase to organic phase:

$$q = \frac{Q_a}{Q_o} \tag{12}$$

$\eta$ is defined as the ratio of the viscosity of the aqueous phase to the organic phase:

$$\eta = \frac{\mu_a}{\mu_o} \tag{13}$$

Among them, $\mu_a$ and $\mu_o$ are the viscosities of aqueous phase and organic phase, respectively.

*3.5.1. Effects of aqueous phase viscosity*

Sontti *et al.* [34] found that the viscosity of aqueous phase can significantly change the shape and size of droplets. Fig. 14 depicts the relationship between the two-phase viscosity ratio $\eta$ and the dimensionless sizes $L_o/W$ and $D_o/W$ when the inlet ratio of MC1 and MC2 is $q = 0.5$ and the aqueous phase flow rate is $Q_a = 42.41$ ml·h$^{-1}$. The flow patterns of MC1 and MC2 are SF and UNI-SF respectively under the studied volume flow ranges. It can be seen that the $D_o/W$ of organic slug in both MC1 and MC2 decreases with the increase of $\eta$. When $\eta = 1.78$, the $D_o/W$ of the slug in MC1 reaches 0.990, while when $\eta = 9.46$, the $D_o/W$ decreases to 0.952. The $D_o/W$ of the slug in MC2 decreases from 0.987 to 0.870. $L_o/W$ also shows a decreasing trend: when $\eta = 1.78$ in MC1, $L_o/W$ is 1.786, and when $\eta = 9.46$, $L_o/W$ decreases to 1.343. Under the same conditions, the $L_o/W$ in MC2 decreases from 2.101 to 1.945. This is because with the increase of $\eta$, the increase of aqueous phase viscosity can inhibit the growth of the slug. It can be seen that $\eta$ has a greater influence on the $L_o/W$ of the slug in MC1 and the $D_o/W$ of the slug in MC2, but has less influence on the $D_o/W$ of the slug in MC1 and the $L_o/W$ of the slug in MC2. This is due to the fact that the friction force on the surface of the insert can restrain the axial shrinkage of the slug, and the insert can also make the slug with fusiform structure more easily covered by the aqueous phase. Therefore, the insert can promote the radial shrinkage of the organic slug when the viscosity of the aqueous phase increases.

*3.5.2. Effects of two-phase flow rate*

In order to prove the effect of two-phase flow on droplet (slug) breakup, and to obtain an effective and universal law, we choose three systems to study: toluene–water, toluene–water + 20% glycerol, toluene–water + 40% glycerol. Change the volume flow rate of

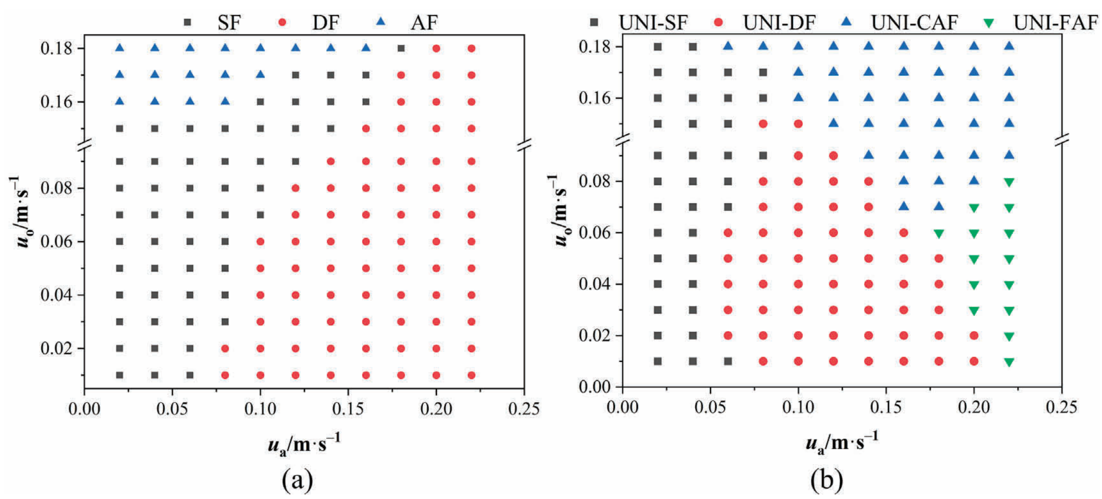


**Fig. 13.** Flow pattern maps: (a) MC1, water–toluene; (b) MC2, water–toluene.

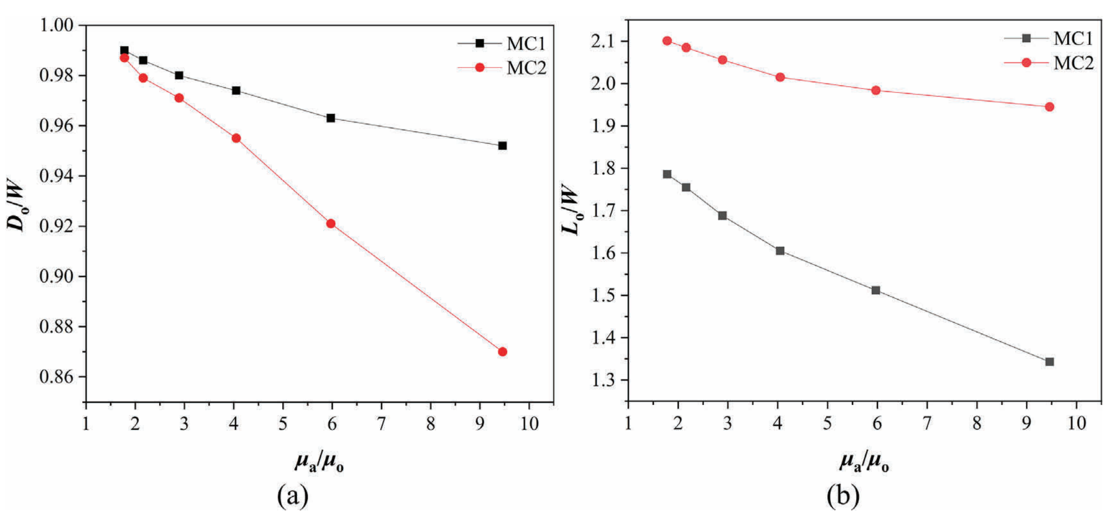


**Fig. 14.** Effects of two-phase viscosity ratio $\eta$ on organic phase dimensionless size: (a) $D_o/W$; (b) $L_o/W$. $q = 0.5$, $Q_a = 42.41$ ml·h$^{-1}$.

the aqueous phase $Q_a$, keep the volume flow rate of the organic phase $Q_o = 21.2$ ml·h$^{-1}$ unchanged, the dimensionless sizes of the flow patterns are studied, and the results are shown in Figs. 15–17.

As shown in Fig. 15, the $L_o/W$ of droplets (slugs) in MC1 decreases with the increase of $Q_a$, because the shear force of aqueous phase relative to the organic phase increases with the increase of the aqueous phase flow rate, thus reducing the $L_o/W$ of the organic phase. When $q$ is smaller, $L_o/W$ decreases faster. When $q$ increases to more than 3, $L_o/W$ decreases slowly, because the increased shear force in the aqueous phase can only regulate the droplet (slug) size to a certain extent. When the size of the droplet (slug) decreases to a certain extent, the shear force of the aqueous phase is no longer dominant, and the size of the droplet (slug) is affected by both the aqueous phase shear force and the two-phase interfacial tension. $D_o/W$ decreases linearly with the increase of $q$. This is because the inertia force of the aqueous phase increases with the increase of $Q_a$, leading to an increase in the thickness of the aqueous liquid film between the organic phase and the channel wall. Through the comparison among the three systems, it can be found that the effect of aqueous phase viscosity on the dimensionless size of flow patterns is obvious, and even if the aqueous phase flow rate increases, the effect of aqueous phase viscosity on the dimensionless size cannot be ignored. However, without insert, the effect of aqueous phase flow rate on $L_o$ is more significant than that of aqueous phase viscosity, while the effect of aqueous phase viscosity on $D_o$ is greater than that of aqueous phase viscosity.

Fig. 16 shows the variation of the dimensionless sizes of UNI-DF in MC2 with the ratio $q$. It can be found that compared with MC1, the $L_o/W$ with insert is relatively larger, and with the increase of $q$, the $L_o/W$ decreases more slowly. But $D_o/W$ is just the opposite. When the insert is available,it decreases rapidly with the increase of $q$, which is similar to the rule in the previous section, because the surface force of the insert has an important influence on the flow pattern size. The shape and channel structure of the deformable slug keep the UNI-DF's $L_o$ within the length range of 1–2 "beads" of the insert. Only when $u_o$ increases to a certain extent relative to $u_a$, the inertia force of organic phase increases, and the influence of insert surface force and aqueous phase shear force is relatively weakened, the droplets can continue to grow. Similarly, under the action of the surface force of the insert, the two ends of the UNI-DF organic phase are not closed, and the slug with fusiform structure is more difficult to stick to the channel wall, but will be covered by the aqueous phase. Therefore, with the increase of

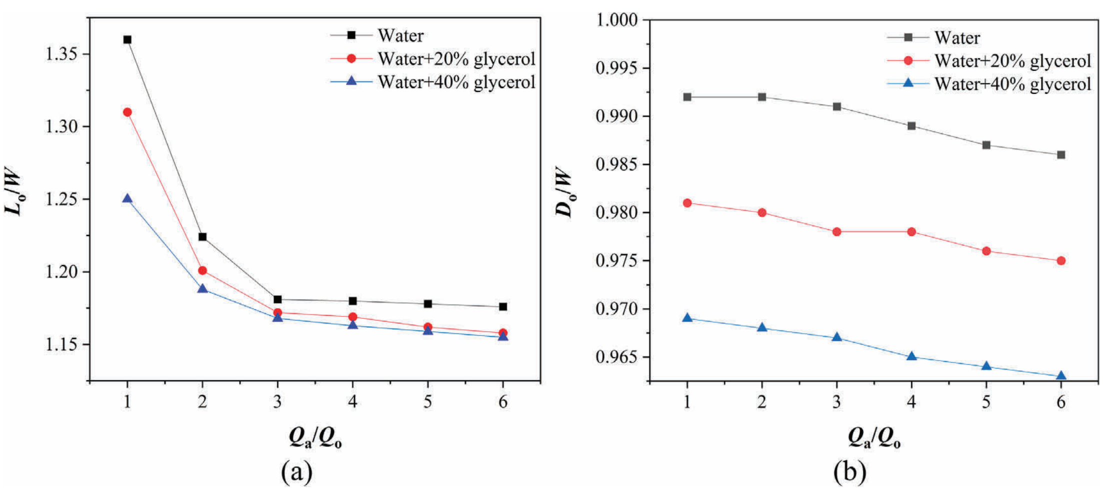


**Fig. 15.** Effects of two-phase flow rate on organic phase dimensionless size in MC1: (a) $L_o/W$; (b) $D_o/W$. $Q_o = 21.2$ ml·h$^{-1}$.

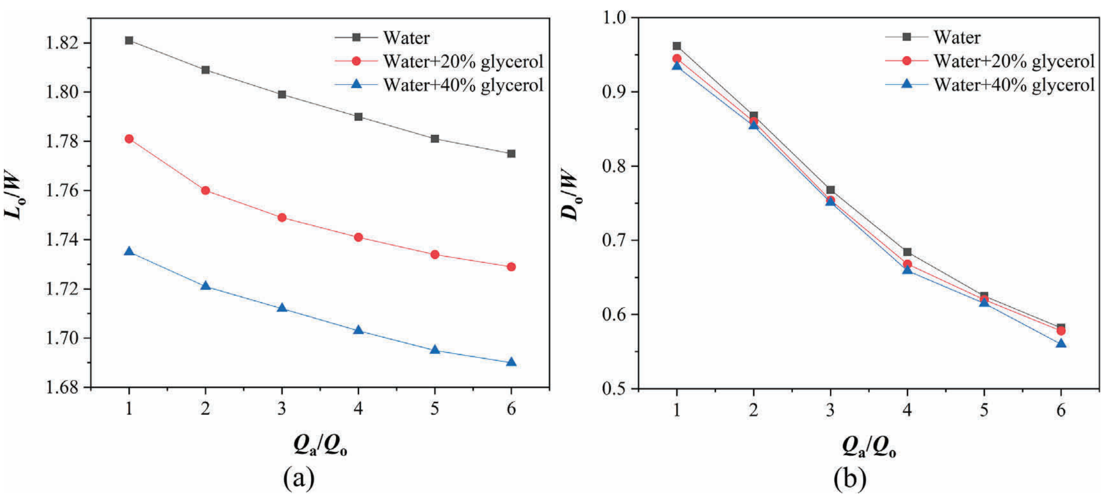


**Fig. 16.** Effects of two-phase flow rate on organic phase dimensionless size in MC2: (a) $L_o/W$; (b) $D_o/W$. $Q_o = 21.2$ ml·h$^{-1}$.

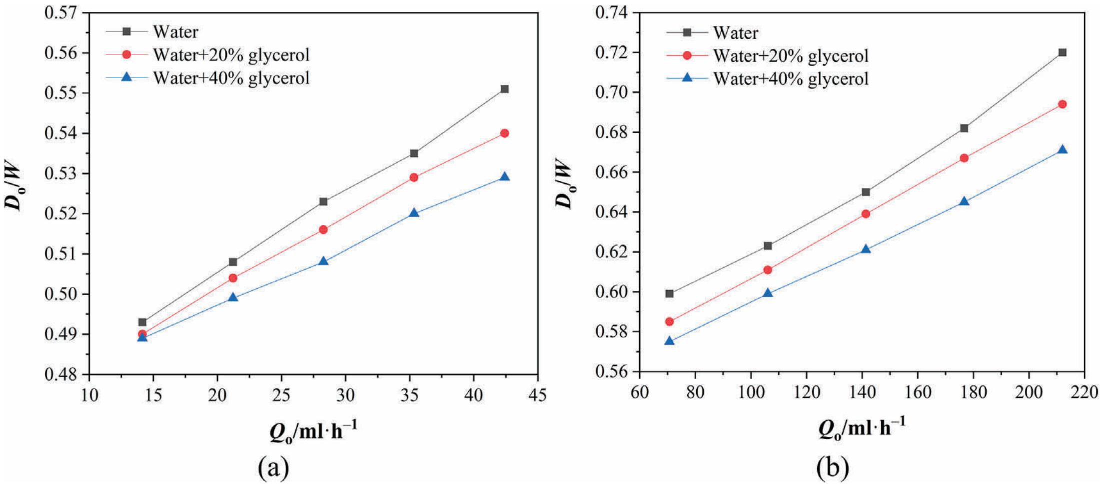


**Fig. 17.** Effects of organic phase flow rate $Q_o$ on annular flow dimensionless radial width $D_o/W$ in MC2: (a) UNI-FAF; (b) UNI-CAF. $Q_a$ = 141.4 ml·h$^{-1}$.

aqueous phase flow rate, the change of the radial size of organic phase is obvious, and the effect of aqueous phase flow rate on the radial size of organic phase is much greater than that of aqueous phase flow rate.

The AF in MC1 is unstable, and it will gradually transition to SF or DF along the channel length direction, because the inertia force of the organic phase cannot maintain the continuity of the organic phase. However, in MC2 the insert makes the annular flow more stable. This part examines the annular flow properties of MC2. Maintains $Q_a$ = 141.4 ml·h$^{-1}$ and the effect of $Q_o$ on the $D_o/W$ in MC2 is shown in Fig. 17. The width of UNI-FAF and UNI-CAF increases with the increase of organic phase flow rate, and there is a linear relationship between $Q_o$ and $D_o/W$ in the measuring range. Compared with the organic flow rate, the viscosity of aqueous phase has little effect on the width of organic phase in annular flow. Although the dominant forces of the two kinds of annular flow are different, the width of annular flow increases linearly with the increase of organic flow rate, which once again shows the fact that the insert can stabilize annular flow under both low-flux and high-flux conditions.

## 4. Conclusions

To recapitulate, in this work, the CFD method is used to study the two-phase flow characteristics in MC1 and MC2. The flow pattern obtained by the simulation is consistent with the experimental graph, which proves that the simulation method is effective. With the change of flow rate, three flow patterns are observed in MC1, namely, DF, SF and AF. While in MC2, four bicontinuous phase flow patterns are observed, namely UNI-DF, UNI-SF, UNI-CAF and UNI-FAF. The velocity vector graph shows that although the droplets (slugs) in MC2 do not break and retract, the insert can promote the formation of recirculation. Pressure monitoring shows that the insert can reduce the pressure drop formed during the formation of the slug. Force analysis shows that the supporting force $F_{N,ins}$ and the friction force $F_{f,ins}$ on the insert surface are the key factors for the formation of the liquid film between the droplets (slugs) to form bicontinuous phase flow patterns. Through the study of the flow pattern map, we can know that the introduction of insert can significantly expand the formation range of annular flow in the flow pattern map. The parameterization study of characteristic size shows that the axial and diameter size of droplet (slug) decreases with the increase of aqueous phase viscosity and the increase of aqueous phase flow rate. The width of annular flow organic phase liquid column decreases with the increase of aqueous phase viscosity, and it increases linearly with the increase of organic phase flow rate.

This work is conducive to solving the contradictory relationship between the mass transfer rate and the phase separation rate in the extraction process. The bicontinuous phase flow pattern means that the insert microchannel has a wide range of applications in wastewater treatment, solvent extraction and other fields. It is necessary to develop new extraction equipment based on bicontinuous phases.

## Data Availability

Data will be made available on request.

## Declaration of Competing Interest

The authors declare that they have no known competing financial interests or personal relationships that could have appeared to influence the work reported in this paper.

## Acknowledgements

The research was financially supported by the National Natural Science Foundation of China (21776180, 22108177), and the Key Research Development Project of Sichuan Province (21ZDYF4086).

## References

[1] K. Jähnisch, V. Hessel, H. Löwe, M. Baerns, Chemistry in microstructured reactors, *Angew. Chem. Int. Ed.* 43 (4) (2004) 406–446.
[2] G.J. Harmsen, Reactive distillation: The front-runner of industrial process intensification, *Chem. Eng. Process. Process. Intensif.* 46 (9) (2007) 774–780.
[3] T.T. Guan, Q. Yan, L.Z. Wan, S.H. Zhang, L.H. Xu, J.L. Wang, J.X. Yun, Liquid–liquid flow patterns and slug characteristics in cross-shaped square microchannel for cryogel beads preparation, *Chem. Eng. Res. Des.* 148 (2019) 312–320.
[4] A. MohdLaziz, K. KuShaari, B. Azeem, S. Yusup, J. Chin, J. Denecke, Rapid production of biodiesel in a microchannel reactor at room temperature by enhancement of mixing behaviour in methanol phase using volume of fluid model, *Chem. Eng. Sci.* 219 (2020) 115532.
[5] M. Kashid, L. Kiwi-Minsker, Quantitative prediction of flow patterns in liquid–liquid flow in micro-capillaries, *Chem. Eng. Process. Process. Intensif.* 50 (10) (2011) 972–978.
[6] J. Jovanović, E.V. Rebrov, T.A.X. Nijhuis, M.T. Kreutzer, V. Hessel, J.C. Schouten, Liquid–liquid flow in a capillary microreactor: Hydrodynamic flow patterns and extraction performance, *Ind. Eng. Chem. Res.* 51 (2) (2012) 1015–1026.
[7] Y.C. Zhao, G.W. Chen, Q. Yuan, Liquid–liquid two-phase flow patterns in a rectangular microchannel, *AIChE J.* 52 (12) (2006) 4052–4060.
[8] S.K.R. Cherlo, S. Kariveti, S. Pushpavanam, Experimental and numerical investigations of two-phase (liquid–liquid) flow behavior in rectangular microchannels, *Ind. Eng. Chem. Res.* 49 (2) (2010) 893–899.

[9] J.H. Xu, G.S. Luo, S.W. Li, G.G. Chen, Shear force induced monodisperse droplet formation in a microfluidic device by controlling wetting properties, *Lab Chip* 6 (1) (2006) 131–136.
[10] T.T. Fu, L.J. Wei, C.Y. Zhu, Y.G. Ma, Flow patterns of liquid–liquid two-phase flow in non-Newtonian fluids in rectangular microchannels, *Chem. Eng. Process. Process. Intensif.* 91 (2015) 114–120.
[11] M. Darekar, K.K. Singh, S. Mukhopadhyay, K.T. Shenoy, Liquid–liquid two-phase flow patterns in Y-Junction microchannels, *Ind. Eng. Chem. Res.* 56 (42) (2017) 12215–12226.
[12] Z. Wu, Z. Cao, B. Sundén, Liquid–liquid flow patterns and slug hydrodynamics in square microchannels of cross-shaped junctions, *Chem. Eng. Sci.* 174 (2017) 56–66.
[13] H. Foroughi, M. Kawaji, Viscous oil–water flows in a microchannel initially saturated with oil: Flow patterns and pressure drop characteristics, *Int. J. Multiph. Flow* 37 (9) (2011) 1147–1155.
[14] W.J. Lan, S.W. Li, G.S. Luo, Numerical and experimental investigation of dripping and jetting flow in a coaxial micro-channel, *Chem. Eng. Sci.* 134 (2015) 76–85.
[15] Y.R. Yin, C.Y. Zhu, T.T. Fu, Y.G. Ma, K. Wang, G.S. Luo, Enhancement effect and mechanism of gas–liquid mass transfer by baffles embedded in the microchannel, *Chem. Eng. Sci.* 201 (2019) 264–273.
[16] R.K. Verma, S. Ghosh, Effect of phase properties on liquid–liquid two-phase flow patterns and pressure drop in serpentine mini geometry, *Chem. Eng. J.* 397 (2020) 125443.
[17] H.C. Lv, Z.R. Yang, J. Zhang, G. Qian, X.Z. Duan, Z.M. Shu, X.G. Zhou, Liquid flow and mass transfer behaviors in a butterfly-shaped microreactor, *Micromachines* 12 (8) (2021) 883.
[18] S. Haase, D.Y. Murzin, T. Salmi, Review on hydrodynamics and mass transfer in minichannel wall reactors with gas–liquid Taylor flow, *Chem. Eng. Res. Des.* 113 (2016) 304–329.
[19] F. Shehzad, I.A. Hussein, M.S. Kamal, W. Ahmad, A.S. Sultan, M.S. Nasser, Polymeric surfactants and emerging alternatives used in the demulsification of produced water: A review, *Polym. Rev.* 58 (1) (2018) 63–101.
[20] A.A. Yagodnitsyna, A.V. Kovalev, A.V. Bilsky, Flow patterns of immiscible liquid–liquid flow in a rectangular microchannel with T-junction, *Chem. Eng. J.* 303 (2016) 547–554.
[21] A. Ghaini, A. Mescher, D.W. Agar, Hydrodynamic studies of liquid–liquid slug flows in circular microchannels, *Chem. Eng. Sci.* 66 (6) (2011) 1168–1178.
[22] M.N. Kashid, D.W. Agar, S. Turek, CFD modelling of mass transfer with and without chemical reaction in the liquid–liquid slug flow microreactor, *Chem. Eng. Sci.* 62 (18–20) (2007) 5102–5109.
[23] A. Abdollahi, S.E. Norris, R.N. Sharma, Pressure drop and film thickness of liquid–liquid Taylor flow in square microchannels, *Int. J. Heat Mass Transf.* 156 (2020) 119802.
[24] Q. Li, P. Angeli, Experimental and numerical hydrodynamic studies of ionic liquid–aqueous plug flow in small channels, *Chem. Eng. J.* 328 (2017) 717–736.
[25] C.W. Hirt, B.D. Nichols, Volume of fluid (VOF) method for the dynamics of free boundaries, *J. Comput. Phys.* 39 (1) (1981) 201–225.
[26] J.U. Brackbill, D.B. Kothe, C. Zemach, A continuum method for modeling surface tension, *J. Comput. Phys.* 100 (2) (1992) 335–354.
[27] R. Gupta, D.F. Fletcher, B.S. Haynes, On the CFD modelling of Taylor flow in microchannels, *Chem. Eng. Sci.* 64 (12) (2009) 2941–2950.
[28] P. Desir, T.Y. Chen, M. Bracconi, B. Saha, M. Maestri, D.G. Vlachos, Experiments and computations of microfluidic liquid–liquid flow patterns, *React. Chem. Eng.* 5 (1) (2020) 39–50.
[29] J.Y. Qian, X.J. Li, Z. Wu, Z.J. Jin, B. Sunden, A comprehensive review on liquid–liquid two-phase flow in microchannel: Flow pattern and mass transfer, *Microfluid. Nanofluid.* 23 (10) (2019) 1–30.
[30] X. Chao, F.S. Xu, C.Q. Yao, T.T. Liu, G.W. Chen, CFD simulation of internal flow and mixing within droplets in a T-junction microchannel, *Ind. Eng. Chem. Res.* 60 (16) (2021) 6038–6047.
[31] A.S. Utada, A. Fernandez-Nieves, H.A. Stone, D.A. Weitz, Dripping to jetting transitions in coflowing liquid streams, *Phys. Rev. Lett.* 99 (9) (2007) 094502.
[32] Z. Cao, Z. Wu, B. Sundén, Dimensionless analysis on liquid-liquid flow patterns and scaling law on slug hydrodynamics in cross-junction microchannels, *Chem. Eng. J.* 344 (2018) 604–615.
[33] Z. Wu, Z. Cao, B. Sunden, Flow patterns and slug scaling of liquid–liquid flow in square microchannels, *Int. J. Multiph. Flow* 112 (2019) 27–39.
[34] S.G. Sontti, A. Atta, Numerical insights on controlled droplet formation in a microfluidic flow-focusing device, *Ind. Eng. Chem. Res.* 59 (9) (2020) 3702–3716.